ELSEVIER

Cement & Concrete Composites 25 (2003) 321–332

Cement & Concrete Composites

www.elsevier.com/locate/cemconcomp

Strength and fracture properties of industrially prepared steel fibre reinforced concrete

M.K. Lee, B.I.G. Barr *

Division of Civil Engineering, Cardiff School of Engineering, Cardiff University, Cardiff, Wales, UK

Received 23 November 2001; accepted 6 June 2002

Abstract

The paper reports on a study of steel fibre reinforced concrete (SFRC) which was prepared using normal industrial mixing, compaction and curing conditions. Both strength (compressive and tensile) and fracture (toughness measurements) characteristics have been investigated with test specimens prepared from 5 m long SFRC piles. The piles contained only steel fibre reinforcement and were manufactured in exactly the same way as ordinary piles.

Slight differences in the tensile strengths (determined via torsion tests) were observed due to the existence of preferential fibre orientation. Flexural tests on notched beams (to evaluate fracture characteristics) produced a much more stable, reproducible, test than that observed for un-notched beams. Hence, it is concluded that the notched beam is a better geometry in terms of test stability and reliability. The results showed that tests specimens taken from industrially prepared SFRC displayed similar characteristics compared to that observed with test specimens prepared under laboratory conditions, with regards to the strength, fracture characteristics and, in particular, the variation observed.

Keywords: Steel; Concrete; Fibre; SFRC; Fracture properties

1. Introduction

Fibre reinforced cement and concrete materials (FRC) have been developed progressively since the early work by Romualdi and Batson [1] in the 1960s. By the 1990s, a wide range of fibre composites and FRC products were commercially available [2] and novel manufacturing techniques were developed for use with high fibre content [3]. In parallel with the commercial development of FRC materials and products, an extensive research programme was undertaken to quantify the enhanced properties of FRC materials and more specifically to allow comparisons to be made between various fibres. Much of this research was published in this Journal.

The enhanced toughness and impact resistance of FRC materials, relative to plain concrete, are two properties which have received considerable attention [4]. Whereas impact tests readily demonstrate the enhanced properties of FRC materials, such tests require sophisticated equipment and instrumentation. Consequently, tests which allow the toughness of FRC materials to be measured have received the greatest attention. Most toughness measurements have been performed on unnotched beams in flexure using a four-point loading arrangement. A review of the general features and methods of interpretation of results from four-point loading tests has been given by Gopalaratnam and Gettu [5]. The review describes the use of various toughness measurements in European, American and Japanese standards. A review of the early development of energy-based dimensionless toughness indices has been given elsewhere [6] and will not be repeated here. Essentially, the practical application of this method began with the introduction of the ACI 544 Toughness Index [7] based on the work of Henegar [8]. ACI Committee 544 defined the toughness index as the ratio of the amount of energy required to deflect a fibre concrete beam by a prescribed amount to the energy required to bring the fibre beam to the point of first crack. Similar notions were used in the development of the ASTM C1018 standard [9] based on the work of Johnston [10]. The main improvement in the ASTM C1018 standard compared with the ACI 544

* Corresponding author. Address: Queen's Building, P.O. Box 925, Newport Road, CF24 OYF Cardifff, UK. Tel.: +44-029-2087-4263; fax: +44-029-2087-4597.

0958-9465/03/$ - see front matter
PII: S0958-9465(02)00060-4

recommendation is that toughness indices (I_5, I_{10}, etc.) are determined for a number of prescribed deflections based on multiples of the first-crack deflection. Further development regarding measuring the toughness of FRC materials have been proposed recently [11].

Most of the research work on steel fibre reinforced concrete (SFRC) has been carried out in testing laboratories under well controlled mixing, compaction, curing and testing conditions [12–16]. This paper reports on a study of SFRC which was prepared using normal industrial mixing, compaction and curing conditions. The study forms part of a Brite-Euram III project involving a number of industrial and academic partners from five EU countries. Both strength (compressive and tensile) and fracture (toughness measurements) characteristics have been investigated in this study. The test specimens were all prepared from 5 m long steel fibre reinforced concrete piles. The piles contained only steel fibre reinforcement and were manufactured in exactly the same way as ordinary piles; the only difference was the addition of the steel fibres to the ready mixed concrete mixer at the site. An important aspect of the study was an investigation of the variability of the test results in comparison with SFRC prepared under laboratory conditions.

2. Test specimens

The test psecimens used in this tudy were taken from SFRC piles, with dimensions of approximately 190 × 190 × 500 mm prepared by Stent Foundations Ltd. The method of manufacture in terms of casting, compaction and curing was identical to that used in the manufacture of normal concrete piles supplied by the company. After fabrication, the pile specimens were transported to Cardiff University where they were stored under ambient laboratory conditions for four weeks before the test specimens were prepared.

2.1. Casting

The concrete mixes were supplied by the Tarmac Topmix ready mix concrete plant based at Pye Bridge, Derbyshire. The mix proportions used for the manufacture of the piles are presented in Table 1. Superplasticiser (Daracem SP1LS) was used to improve the workability of the mix to facilitate the addition of fibres. The superplasticiser is based on the soluble salt of a polymeric naphthalene sulphonate. The steel fibres (Dramix RC60/65 BN steel fibres, supplied by N.V. Bekaert S.A.) were hooked and collated with a length of 60 mm and aspect ratio of 65. A total of 50 kg/m^3 of fibres were added into the concrete mix. Concrete cubes were prepared from the concrete mix before and after the addition of the steel fibres. After placing, a poker vibrator was used as a means of compaction.

Table 1
Mix details

Material	Quantity (kg/m^3)
Cement	350
Sand	853
Gravel (10 mm)	1040
Water	174
Daracem superplasticiser	3.50

Cube compressive strength tests were carried out (by Stent Foundations Ltd.) on the concrete samples at various ages and the results are shown in Fig. 1 [17]. It is apparent that there is no significant difference between the cube compressive strength of the samples with and without fibre reinforcement. However, firm conclusions regarding the difference in strength should not be drawn due to the relatively high variation in the individual cube results obtained up to 28 days. This is as expected and is similar to that observed during laboratory testing of SFRC.

2.2. Test specimen preparation

The piles were cut into segments of approximately 600 mm in length. Four beam specimens were extracted from each pile as illustrated in Fig. 2. Subsequently, six cylinders were cored, using a diamond core drill, from the remaining central segment of the pile. These cores

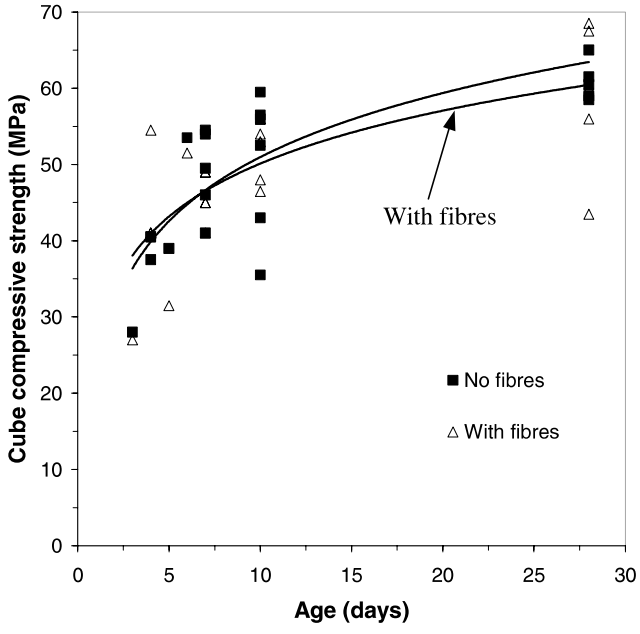

Fig. 1. Development of cube compressive strength with age (first 28 days).

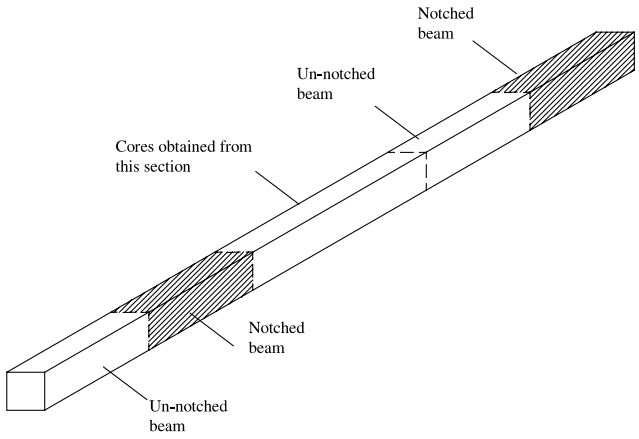

Fig. 2. Schematic view of pile divided into four beams and a central section from which cores were obtained.

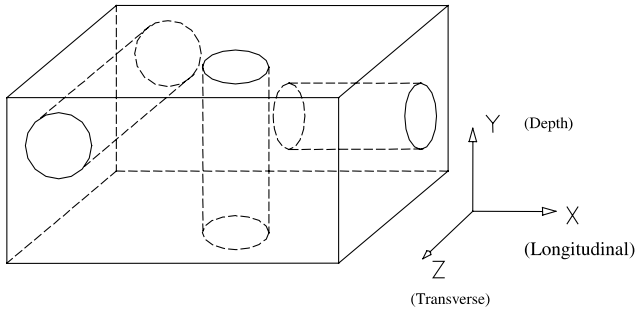

Fig. 3. Schematic view of cores obtained in three orthogonal directions.

were cut in three orthogonal directions as shown in Fig. 3. The coring of the longitudinal cores was carried out away from the edges in order to reduce edge effects. All cores were cut using the same coring bit which gave core diameters in the range of 103–105 mm. The length of each core was limited to 190 mm which was the maximum possible in two of the directions and the same length was adopted for the longitudinal cores.

Half the beams were notched with an Errut masonry saw whilst the other half were left un-notched. The notches were prepared in such a way that the test specimens were left with a 160 mm ligament. The reason for prescribing this ligament length is so that the notched cross-section would be geometrically similar to the beam test proposed by RILEM TC-162 TDF [11].

3. Test programme

The torsion tests were carried out in a 600 kN servo-hydraulic Avery-Denison machine under stroke control at a prescribed rate of 10 μm/s. The torsion test set-up,

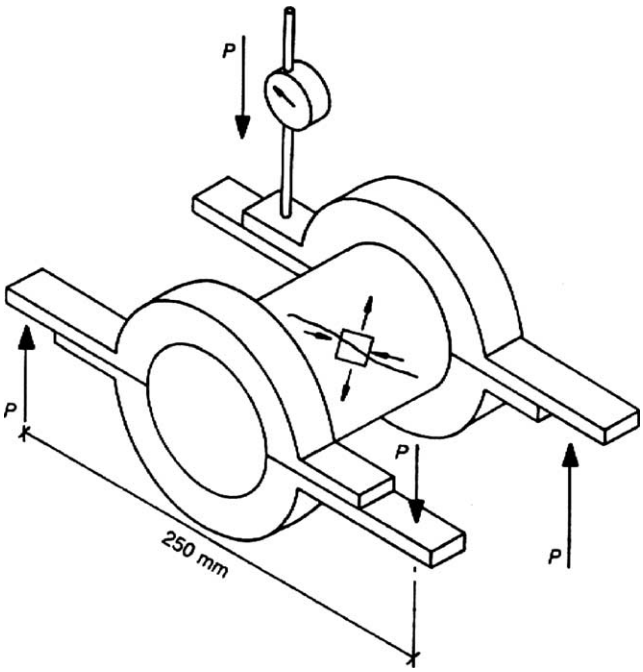

Fig. 4. Schematic view of torsion test arrangement (after [18]).

as shown in Fig. 4, is identical to that reported by Norris et al. [18]. Both ends of the cored cylinder were first lacerated to produce a rough surface to provide a good bond with the split collars. The collars were attached, using a two-component adhesive, to both ends of the cored cylinders. Upward reactions are provided by two supports, whereas a third provides a downward reaction. At the free end, a load P is applied thus producing reactions of P at the other three supports. An LVDT was used to measure the rotation of the cylinder over a gauge length of 90 mm. A specially made circular frame was used to hold the LVDT in place. The distance of the LVDT from the centre of the cylindrical test specimen is 125 mm.

The distance between the pairs of loads on the split collar is 250 mm, which leads to a torque of $0.25P$. The load and LVDT readings were recorded automatically by a Personal Computer at a rate of 20 Hz.

The beams, notched and un-notched, were tested in a 250 kN closed-looped servo-hydraulic Dartec 9600 machine. For the un-notched beams, the average mid-span deflection was used as the feedback signal whereas the notched beams used the crack mouth opening displacement (CMOD) as the feedback signal. Knife-edges were installed using plastic padding at the bottom of the notched beams to hold the CMOD clip gauge. The strain rate adopted for the beam tests was 200 μm/min. Schematic diagrams illustrating the test set-ups are given in Figs. 5 and 6. Holes were introduced, using a masonry drill, at mid-height of the beams at the supports to install screws to hold a yoke arrangement. This yoke

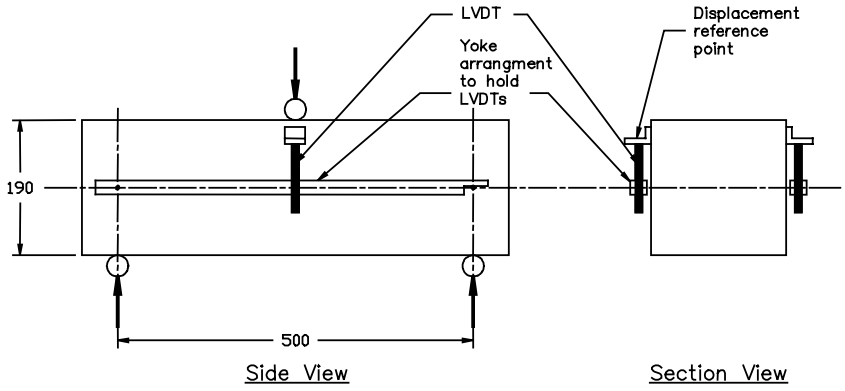

Fig. 5. Test set-up for un-notched beam specimen.

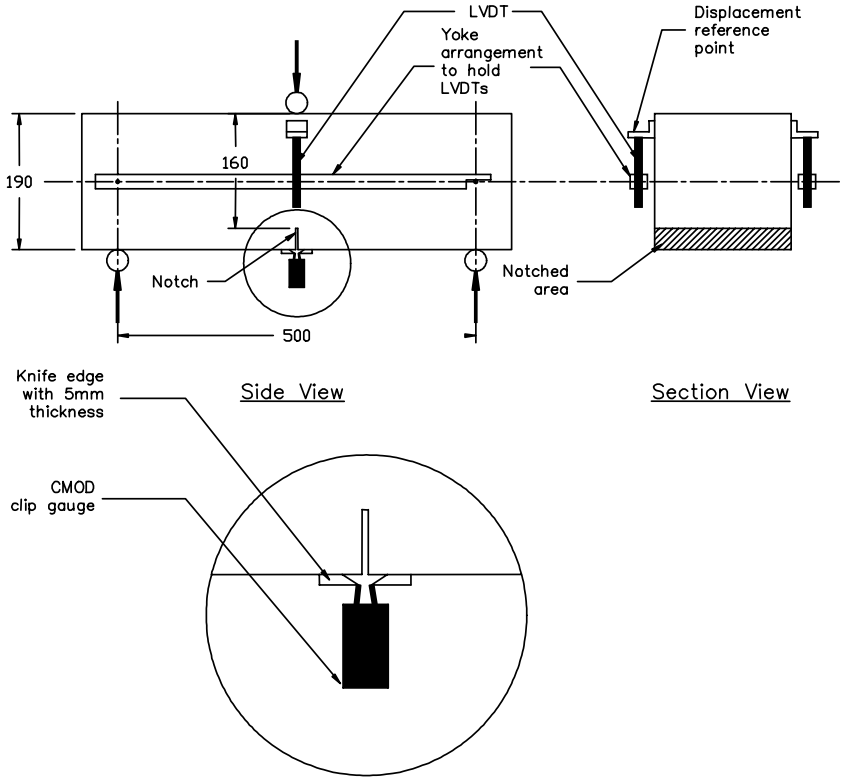

Fig. 6. Test set-up for notched beam specimen.

arrangement held LVDTs so that deflections were measured directly from the specimens. Load, mid-span deflections and CMOD readings (for the notched beam) was recorded onto a floppy disc every 2 s.

4. Methods of analysis

Several strength and toughness parameters were evaluated from the test results. From the torsion test, an indirect tensile strength and Young's modulus were evaluated. On the other hand, from the beam tests, flexural tensile strength and toughness measurements were calculated. In addition, fracture resistance curves were determined from the notched beam tests.

4.1. Indirect tensile strength from torsion test

If a cylinder is subjected to torsion alone, then it is in a state of pure shear as shown in Fig. 7a. This results in equal tensile and compressive stresses at 45° to the longitudinal axis (principal stresses) of the cylinder as

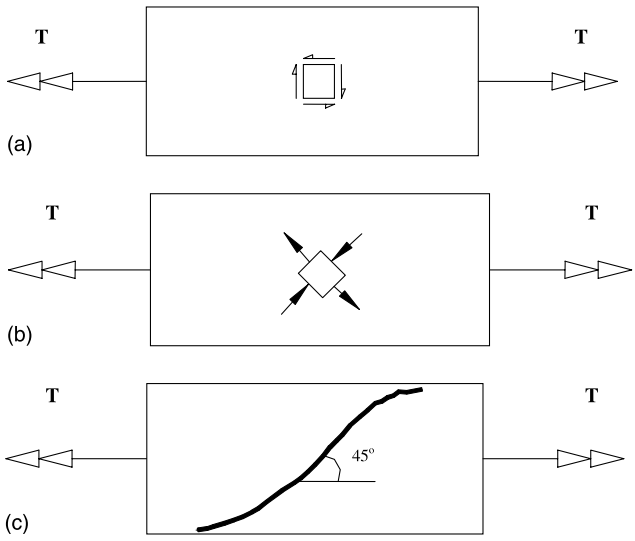

Fig. 7. Stress distribution and typical failure mode in cores due to the applied torque, T. (a) Shear stress distribution due to torque, T. (b) Principal stress distribution (tension and compression) due to T. (c) Typical failure mode with initial crack at 45° to horizontal axis.

shown in Fig. 7b. Materials that are weak in tension will fail by cracking along a 45° helical surface as shown in Fig. 7c. As concrete is weak in tension, it is expected that this would be the mode of failure in a torsion test on the SFRC specimens.

Indirect tensile strength values can be calculated from the torsion test results by using classical solid mechanics. Several assumptions were made when deriving the tensile strength values:

- The specimen behaves elastically.
- Uniform twisting occurs along the cylinder.
- The cross-sections remain planar and the radii remain straight.
- The shear stress is maximum at the circumference and zero at the centre, and the shearing stresses vary linearly over the cross-section.

For a linear-elastic material, the solution for the torque-twist relationship is given by [19]:

$$\frac{T}{J} = \frac{\tau}{r} = \frac{G\Phi}{L} \tag{1}$$

where T is the torque applied, J is the polar second moment of area of the cross-section, τ is the shear stress at radius r, r is any given radius, G is the shear modulus and L is the length over which rotation Φ is measured.

From Eq. (1), the following expression may be obtained:

$$\tau = \frac{\mathrm{Tr}}{J} \tag{2}$$

The value of τ in Equation (2) is a measure of the tensile strength of the material because the SFRC matrix has a low tensile strength and consequently cracking will be initiated due to the failure of the material in tension.

In addition, the shear modulus, G, can be calculated by re-arranging Eq. (1):

$$G = \frac{TL}{J\Phi} \tag{3}$$

The value of rotation Φ can be calculated from the LVDT measurement carried out during the test. As mentioned before, a single LVDT was used to record displacements over a gauge length of 90 mm and at a distance of 125 mm from the centre of the test specimen. By assuming small angle rotations, Φ can be calculated.

The Young's modulus, E, can be calculated by using the following relationship between E and G:

$$G = \frac{E}{2(1+v)} \tag{4}$$

where v is Poisson's ratio, assumed to be 0.2. (This assumed value of 0.2 for v is typical of that reported in the literature e.g. by Kliszczewicz and Ajdukiewicz [20] and the FIP/CEB report for high strength concrete [21]).

Note that for the calculation of E, the peak load recorded was not used. This is due to the non-linearity of the response as the cracking strength is approached caused by microcracking. Instead, an arbitrary load level of 40% of the peak load in the elastic regime is used for calculation of the value of E.

4.2. Flexural tensile strength

Flexural tensile strength values were calculated from the load at the limit of proportionality using simple elastic analysis. The assumed stress distribution for the un-notched and notched beams at the point of cracking is illustrated in Fig. 8. The assumptions made are:

- The beams behaves elastically.
- The extreme fibre of the concrete surface in tension is just at the point of cracking.
- The Young's modulus in compression is equal to that in tension.

It is acknowledged that this is a simplified view and not entirely valid due to the non-linear nature of concrete under loading.

For the un-notched beam, the flexural tensile strength, $\sigma_{\mathrm{fl,un}}$, is calculated as:

$$\sigma_{\mathrm{fl,un}} = \frac{3F_{\mathrm{u}}L}{2bh^2} \tag{5}$$

whereas, for the notched beams, the flexural tensile strength, $\sigma_{\mathrm{fl,n}}$, is given by:

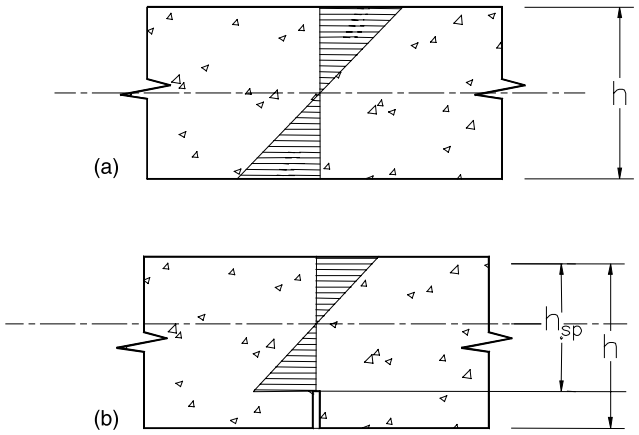

Fig. 8. Assumed stress distribution at cracking. (a) Un-notched beam specimen and (b) notched beam specimen.

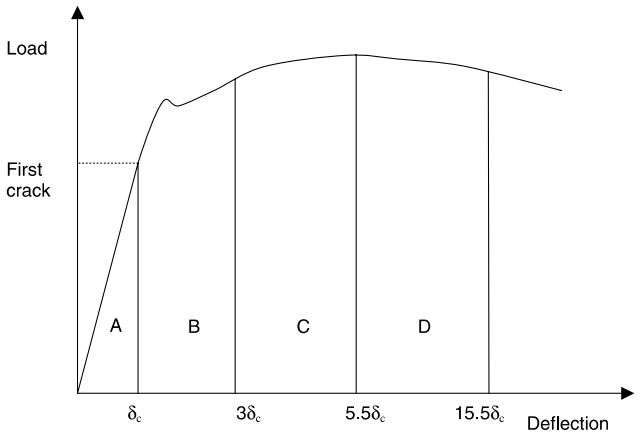

Fig. 9. Areas under the load–deflection curve used to determine toughness indices (after [9]).

$$\sigma_{fl,n} = \frac{3F_u L}{2bh_{sp}^2} \tag{6}$$

where F_u is the load at the end of the limit of proportionality, L is the test span, b is the width of the beam, h is the total depth of the beam and h_{sp} is the ligament depth. The load, F_u, is determined according to the RILEM recommendation [11].

4.3. Toughness indices

To evaluate the toughness of the beam specimens, toughness indices calculated in accordance with ASTM C1018 [9] were used. For the work presented here, the three well established toughness indices were calculated i.e. I_5, I_{10} and I_{30}. In essence, the indices are expressed as the areas under the load–deflection curve at set multiples of the first crack deflection, divided by the area to the first crack deflection.

Fig. 9 illustrates the method by which the toughness indices were calculated. Area A represents the energy required to cause the concrete matrix to crack and the behaviour changes from an elastic one to a non-linear behaviour. On the other hand, areas B, $(B + C)$ and $(B + C + D)$ represents the energy absorbed to cause the specimen to deflect to reach deflections of $3\delta_c$, $5.5\delta_c$ and $15.5\delta_c$ respectively (where δ_c = deflection at first crack). In this investigation, δ_c, was determined by eye from the P–δ (or P–CMOD) curves. Thereafter, the calculation of the relevant toughness indices is straightforward.

By referring to Fig. 9, the toughness indices are calculated as follows:

$$I_5 = \frac{A + B}{A} \tag{7}$$

$$I_{10} = \frac{A + B + C}{A} \tag{8}$$

$$I_{30} = \frac{A + B + C + D}{A} \tag{9}$$

Note that the ASTM C1018 is drawn up for a certain test geometry and configuration. However, the concept of calculating toughness indices given by ASTM is only used as a tool to carry out a quantitative comparison for the work presented here.

4.4. Proposed rilem design parameters

As an alternative to the ASTM C1018 approach, the design parameters as defined by RILEM TC 162-TDF [11] were also calculated here as a basis for comparison. The procedure involved in calculating the parameters f_{fct}, f_{eq2} and f_{eq3} is illustrated in Fig. 10, which also defines the three parameters.

Although, the calculation procedure for the un-notched and notched beams are identical, the value of the ligament depth is different. The ligament depth, h_{sp}, for the un-notched and notched beams is 190 and 160 mm respectively.

For results analysed using the P–CMOD curves, the procedure is the same as that used on the F–δ curves (as shown in Fig. 10). However, instead of using δ_{Fu} as defined by Fig. 10, a value of $CMOD_{Fu}$ was evaluated from the P–CMOD. The corresponding CMOD values used to calculated f_{eq2} and f_{eq3} are $CMOD_{Fu} + 0.65$ mm and $CMOD_{Fu} + 2.65$ mm.

4.5. Fracture resistance curves

In addition to the investigations carried out above, the data for the notched beams were analysed from a fracture mechanics point of view. Fracture resistance curves (R-curves) were produced where the stress intensity factor, K_I, at the tip of the effective crack is plotted as a function of the effective crack length, a_{eff}. The concept of the effective crack length is used because, for laboratory-sized specimens, the size of the fracture

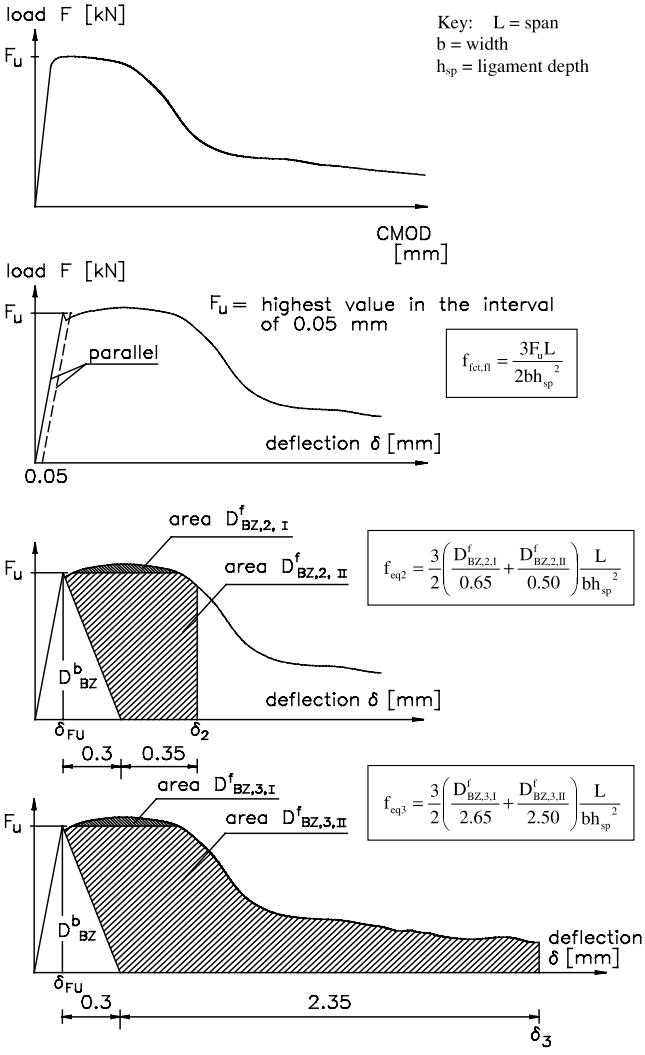

Fig. 10. Diagrams showing method of calculating RILEM design parameters i.e. f_{fct}, f_{eq2} and f_{eq3} (after [11]).

process zone is significant. This leads to a deviation from the straightforward linear elastic fracture mechanics solution.

R-curves have been used by numerous research workers to characterise stable crack growth for rocks, concrete and other cementitious composites [22–26]. Additionally, it has been used to provide a measure for the toughening effect provided by fibre addition [24,27]. The *R*-curve concept however is not, strictly speaking, a material property as it has been shown to depend on the specimen size and geometry [26,28,29]. The *R*-curve concept is used in this work solely to quantify the fracture behaviour of the test specimens.

The effective crack length, a_{eff}, was calculated using the compliance calibration technique, based on the *P*–CMOD curves. Subsequently the fracture toughness, K_I, based on the effective crack length was calculated. This concept is illustrated in Fig. 11.

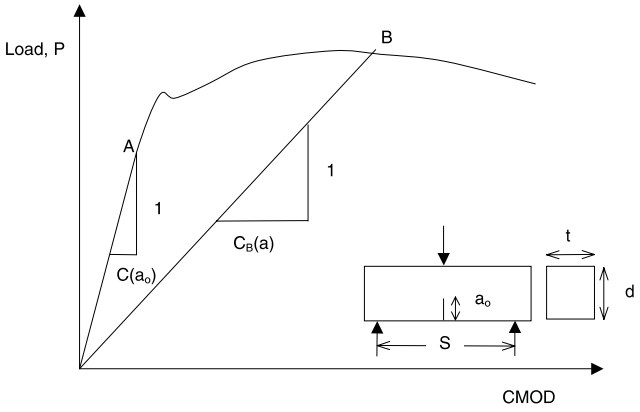

Fig. 11. Compliance calibration based on the *P*–CMOD curve (after [30]).

From linear elastic fracture mechanics (LEFM), the CMOD is given by [30]:

$$\text{CMOD} = \frac{6\sigma a}{E} f(\alpha(a)) \tag{10}$$

where σ is the stress and a is the crack length.

The expression $\alpha(a)$ takes into account the fact that the CMOD is not measured directly at the bottom fibre of the beam, and is given by:

$$\alpha(a) = \frac{a + d_0}{d + d_0} \tag{11}$$

where a is the crack length, d is the beam depth and d_0 is the depth from the bottom of the beam at which the CMOD is measured (for this work, $d_0 = 5$ mm).

The geometrical function, $f(\alpha(a))$ for a specimen with span to depth ratio (S/d) of 2.5 is given by:

$$f(\alpha(a)) = \frac{1.73 - 8.56(a/d) + 31.2(a/d)^2 - 46.3(a/d)^3 + 25.1(a/d)^4}{(1 - a/d)^{3/2}} \tag{12}$$

For a beam under three point loading:

$$\sigma = \frac{3PS}{2d^2 t} \tag{13}$$

where P is the applied load, S is the span, d is the depth and t is the specimen thickness.

Applying Eqs. (11) and (12) at point A and B (refer to Fig. 11) gives:

$$E = \frac{6a_0 S}{C(a_0)d^2 t} f(\alpha(a_0)) = \frac{6a_{\text{eff}} S}{C(a_{\text{eff}})d^2 t} f(\alpha(a_{\text{eff}})) \tag{14}$$

Rearranging Eq. (14) gives:

$$a_{\text{eff}} = a_0 \frac{C(a_{\text{eff}}) f(\alpha(a_0))}{C(a_0) f(\alpha(a_{\text{eff}}))} \tag{15}$$

Using Eq. (15) through a process of trial and error, the value of a_{eff} is calculated.

The stress intensity factor, K_{I} is given by [30]:

$$K_{\text{I}}(a) = \sigma\sqrt{\pi a}g(a/d) \tag{16}$$

For the loading configuration considered, the geometrical factor $g(a/d)$ is:

$$g(a/d) = \frac{1 - 2.5(a/d) + 4.49(a/d)^2 - 3.98(a/d)^3 + 1.33(a/d)^4}{(1 - a/d)^{3/2}} \tag{17}$$

From the calculated values of K_{I} and a_{eff}, fracture resistance curves may be plotted (K_R-curves).

5. Results and discussion

5.1. Torsion test

Fig. 12 shows a typical response of a cylinder specimen during the torsion test. The response is approximately linear during the initial part of the test. At peak load, it can be observed that a crack is formed approximately 45° to the longitudinal axis i.e. perpendicular to the direction of the maximum tensile stress. The presence of fibres prevents the specimen from failing completely and hence the post-peak response could be recorded. This differs from the response of plain concrete specimens, where total rupture occurs and no post-peak response can be measured using this simple torsion test set-up [18].

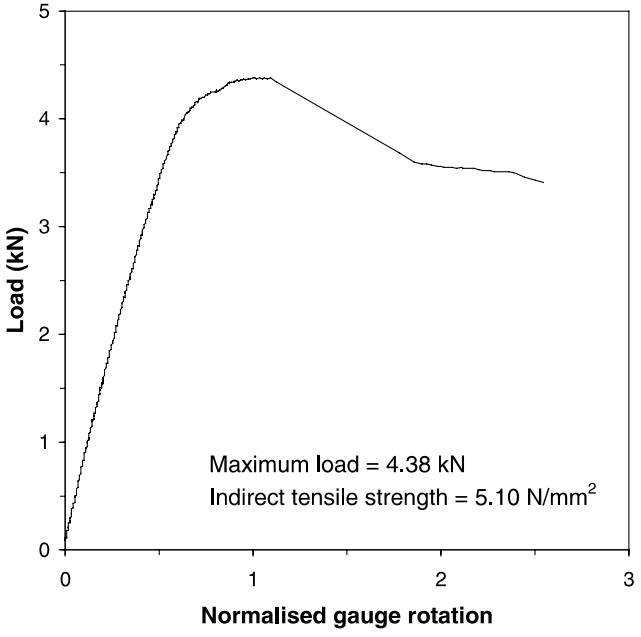

Fig. 12. A typical response for a torsion test specimen (example taken from results for specimen AX1).

Table 2
Torsion test results

Ref. No.	Max. load (kN)	Max. load deflection (mm)	Young's Modulus, E (GPa)
Cylinders cored in the X-axis direction			
AX1	4.38	0.119	39.6
AX2	4.11	0.097	41.7
BX1	4.05	0.087	37.4
BX2	4.42	0.098	40.0
CX1	3.86	0.097	40.9
CX2	4.53	0.112	33.5
DX1	4.04	0.107	37.8
DX2	3.99	0.112	39.1
Average	4.17	0.104	38.8
V (%)	(5.73)	(10.2)	(6.64)
Cylinders cored in the Y-axis direction			
AY1	4.71	0.097	39.6
AY2	4.12	0.097	39.8
BY1	4.29	0.082	43.5
BY2	4.31	0.092	38.9
CY1	4.52	0.107	35.3
CY2	4.05	0.100	35.3
DY1	4.16	0.085	39.7
DY2	4.50	0.105	37.9
Average	4.33	0.096	38.8
V (%)	(5.27)	(9.32)	(6.89)
Cylinders cored in the Z-axis direction			
AZ1	4.02	0.107	40.7
AZ2	3.94	0.091	40.0
BZ1	4.36	0.093	42.3
BZ2	4.25	0.121	39.9
CZ1	4.27	0.128	37.1
CZ2	3.83	0.096	39.8
DZ1	4.17	0.092	40.6
DZ2	4.11	0.102	37.1
Average	4.12	0.104	39.7
V (%)	(4.36)	(13.5)	(4.48)

The result for all the cylinder specimens are tabulated in Tables 2 and 3. The method employed in calculating the Young's modulus, E, provides satisfactory results which are close to the expected values. More significantly, the scatter of the results are generally below 10% implying that this could be a robust method for quantifying E.

Table 3 shows the indirect tensile strength calculated for the specimens in the three different directions. Once again, the scatter of the results is limited in range, with the coefficient of variation being generally within 5%. The tensile strength values obtained in the X-axis and Z-axis are in close agreement with one another. On the other hand, the Y-axis shows a slightly higher tensile strength. This is as expected when the orientation of the fibres during compaction is taken into account [31,32].

Table 3
Indirect tensile strength values for the *X*-, *Y*- and *Z*-axis

Beam ref.	Indirect tensile strength (MPa)		
	X-axis	*Y*-axis	*Z*-axis
A-1	5.10	5.49	4.68
A-2	4.79	4.80	4.59
B-1	4.72	5.00	5.08
B-2	5.15	5.02	4.95
C-1	4.50	5.27	4.98
C-2	5.28	4.72	4.46
D-1	4.71	4.84	4.86
D-2	4.65	5.24	4.79
Average	4.86	5.05	4.80
V (%)	(5.73)	(5.27)	(4.36)

It has been shown by various research workers that compaction during the fabrication of SFRC specimens influences the fibre distribution and orientation [33–36]. It has been observed that the vibration of SFRC tends to orientate the fibres towards horizontal planes [33, 35] and the level of workability influences the rate of fibre settlement [34]. Hence, preferential fibre alignment and orientation could be the cause of the higher strength being observed in the *Y*-direction. However, the difference between the tensile strength for all three axis is not very large since the action of the fibres do not play a significant role in the initial cracking of the specimen. The cracking of the matrix would be the dominant factor at this stage [37]. Nonetheless, the small differences observed between the tensile strength values do indicate that there is a slight contribution by the fibres during the process of crack initiation.

Overall, the low variability of the indirect tensile strength results reflects the robustness of the torsion test. It is therefore possible to obtain values of tensile strength and even the modulus of elasticity for use with

Table 4
Toughness test results for un-notched beams (Panel A), notched beams calculated using P–δ curves (Panel B) and notched beams calculated using P–CMOD curves (Panel C)

Beam ref.	First crack load (kN)	First crack deflection (mm)	I_5	I_{10}	I_{30}	f_{fct} (N/mm^2)	f_{eq2} (N/mm^2)	f_{eq3} (N/mm^2)
Panel A								
A1	49.5	0.119	7.30	16.1	47.6	5.55	6.58	5.89
A4	46.8	0.080	5.89	12.4	37.7	5.25	5.24	4.95
B2	46.9	0.091	7.11	15.6	47.2	5.27	6.88	6.08
B3	45.6	0.074	2.92	6.38	22.1	5.13	2.21	2.85
C1	39.8	0.030	2.22	4.22	17.0	4.47	3.17	3.75
C4	49.8	0.077	5.16	10.8	33.6	5.59	5.47	4.89
D2	48.1	0.098	4.90	9.35	25.1	5.40	4.07	3.57
D3	Damaged							
Average	46.6	0.081	5.07	10.7	32.9	5.24	4.80	4.57
V (%)	(7.23)	(33.6)	(38.2)	(41.6)	(36.6)	(7.23)	(36.1)	(26.7)
Panel B								
A2	30.3	0.045	3.70	7.49	24.0	4.80	5.81	5.74
A3	34.8	0.079	4.83	9.63	29.1	5.50	3.76	3.82
B1	31.7	0.080	5.91	12.6	38.2	5.02	4.79	4.42
B4	29.5	0.081	6.06	12.5	37.5	4.67	4.26	3.98
C2	30.4	0.086	6.05	13.5	47.3	4.82	6.34	6.89
C3	35.5	0.082	6.85	15.0	45.0	5.62	5.76	5.16
D1	33.4	0.095	5.55	12.1	41.3	5.29	6.68	7.02
D4	31.2	0.044	3.03	6.10	19.7	4.94	6.26	6.61
Avg	32.1	0.074	5.25	11.1	35.3	5.08	5.46	5.46
V (%)	(6.88)	(25.7)	(24.8)	(27.6)	(28.2)	(6.88)	(19.5)	(23.9)
Panel C								
A2	30.3	0.047	4.73	8.98	29.1	4.80	5.68	5.91
A3	34.8	0.032	3.69	6.98	18.9	5.50	3.72	3.95
B1	31.7	0.037	3.88	7.61	22.6	5.02	4.78	4.64
B4	29.5	0.036	4.12	7.77	22.4	4.67	4.23	4.10
C2	30.4	0.052	4.05	8.43	28.3	4.82	6.06	6.93
C3	35.5	0.032	4.68	9.14	28.3	5.62	5.69	5.35
D1	33.4	0.061	3.81	7.79	25.8	5.29	6.41	7.15
D4	31.2	0.054	3.84	7.76	26.0	4.94	6.03	6.65
Avg	32.1	0.044	4.10	8.06	25.2	5.08	5.32	5.59
V (%)	(6.88)	(25.2)	(9.63)	(9.13)	(14.2)	(6.88)	(18.2)	(22.8)

the stress-crack opening relationship in modelling. RILEM TC 162-TDF has proposed a uniaxial tensile test method for obtaining the stress-crack opening relationship, however, it is recommended that the tensile strength value be evaluated independently [38]. The torsion test could be such an alternative method.

5.2. Beams under three-point bending

Table 4 (Panels A–C) show the results for the beams tested under three-point bending. Results for the notched beams were analysed via the use of the P–δ and the P–CMOD curves and are given in Table 4 (Panels B and C) respectively. These tables show that the variability of results calculated from the un-notched beams is higher than that from the notched beams. During the tests, it was observed that the notched beams gave a more stable response.

On the other hand, for the un-notched beams, a number of specimens had to be tested in two stages. When cracking first occurred, the test machine unloaded since there was an abrupt change in the deflection. Consequently, for these situations, the tests could not be carried out as one continuous test.

Fig. 13a and b compare the results between the notched and un-notched beams. The P–δ curves are given in terms of 95% confidence interval envelopes. The variability for the un-notched beams is significantly higher than those of the notched beams in the initial stages of the test. This leads to the conclusion that the notched beam would be more suitable for use as a standard test.

The variation in the results for the notched and un-notched beams approaches the same level after a mid-span deflection of approximately 1.2 mm. At advanced stages of cracking ($\delta > 1.25$ mm), the coefficient of variation is of the order of 20%. This is similar to the findings reported in [39] for SFRC with the same fibre dosage. Hence, the industrially prepared specimens display similar fracture characteristics in terms of the scatter of results. This leads to the conclusion that full-scale industrial preparation does not significantly change the statistical distribution of the results relative to that observed in laboratory tests.

Notice that only a comparison between the variation observed in the laboratory prepared specimens and industrially prepared specimens has been carried out. No comparison has been carried out between the actual P–δ curves i.e. load levels at various mid-span deflections. This is because the tested samples cannot be compared directly with the samples tested in accordance with the RILEM recommendations. Although steps have been taken to maintain geometrical similarity, the actual dimensions are different.

The variability of the results calculated from the P–CMOD is the lowest and indicates the suitability of the

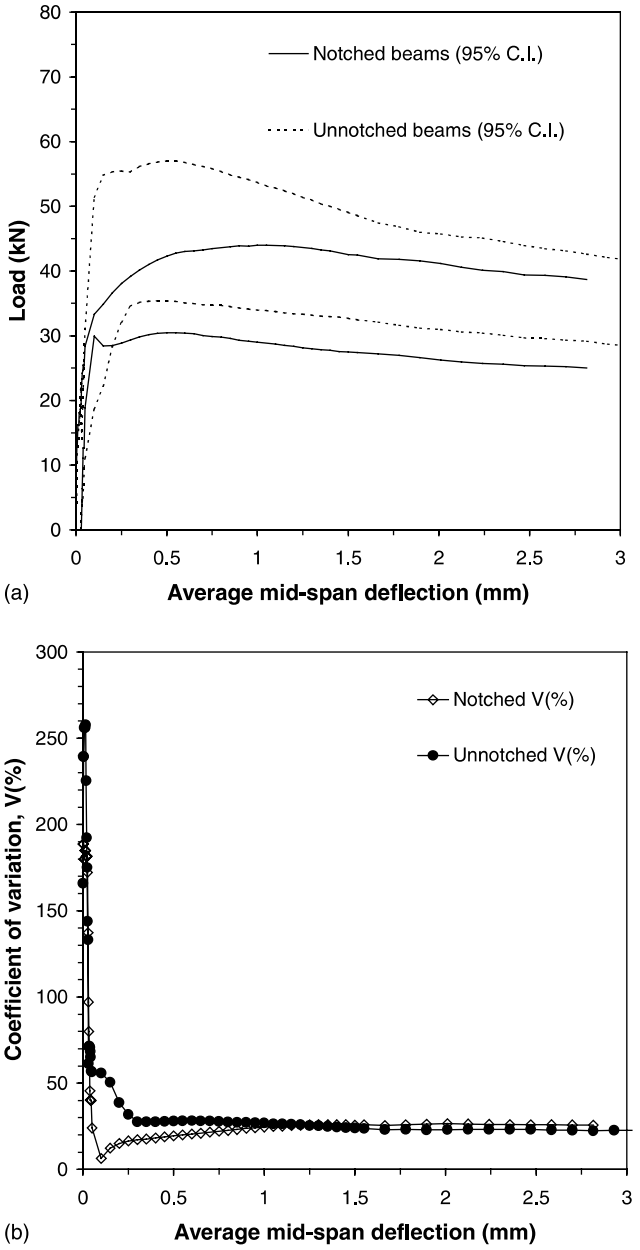

Fig. 13. Comparison between the load-average mid-span deflection curves of the notched and un-notched beam specimens. (a) Upper and lower limit (at 95% confidence interval) of the P–δ curves for the beam specimens. (b) Variation of the P–δ curves for the beam specimens vs average mid-span deflection.

P–CMOD for the calculation of toughness and other parameters as indicated by several other researchers [40–43].

Fig. 14 shows a typical K_R-curve calculated for the notched SFRC beams. Fig. 15 shows all the calculated K_R-curves including the average curve. The curves show an increasing trend with no indication of reaching a plateau. This gives an indication of a significant fracture process zone in relation to the specimen dimensions.

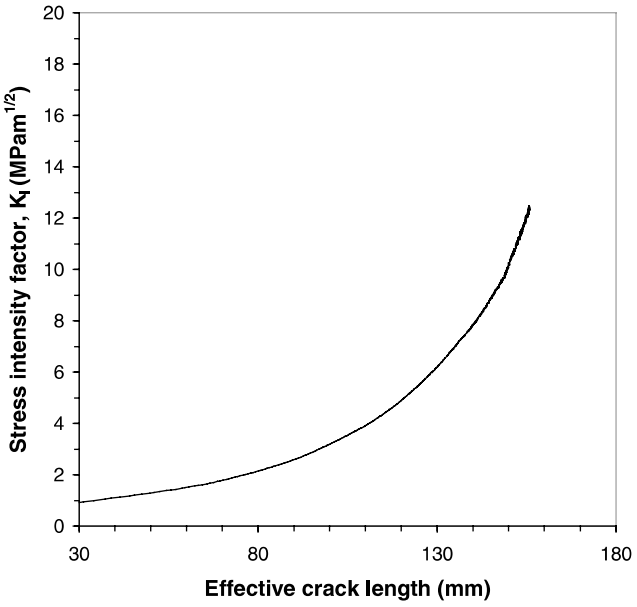

Fig. 14. A typical K_R-curve for the notched SFRC beams plotted as a crack growth resistance curve (K_I vs a_{eff}).

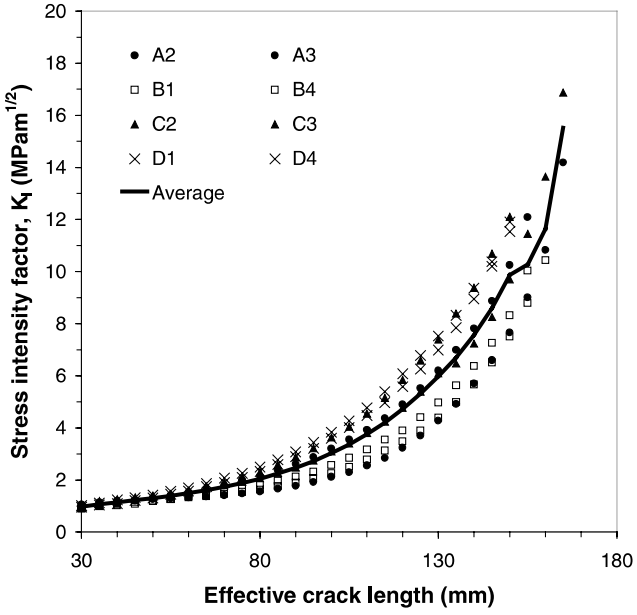

Fig. 15. K_R-curves for all the notched SFRC beams.

6. Conclusions

The torsion test results showed that the test is a good indirect method to determine the tensile strength and the modulus of elasticity of fibre reinforced concrete. The method is relatively straightforward and statistical analysis showed that the test method is robust and reproducible. It was observed that there was a slight difference in the tensile strengths obtained, particularly in cores obtained from the in-depth direction, due to the existence of preferential fibre orientation.

From the tests carried out on the beam specimens, it is evident that notched beams produce a much more stable test and allows the test to be conducted continuously at the prescribed strain rate (200 μm/min for this work). The variation in the results for the notched beams are found to be significantly lower than the un-notched beams in the initial stages of loading and in the initial post-peak regime. This variation, however, approaches a similar level in the advanced stages of cracking. Hence, it can be concluded that the notched beam is a better geometry in terms of test stability and reliability.

At advanced stages of cracking, the variation in the results is similar to that observed for laboratory prepared specimens (similar type of SFRC) at approximately 20%. Therefore, industrially prepared specimens display similar fracture characteristics with regards to the variation observed. However, further work in this area is recommended before drawing firm conclusions.

The *P*–CMOD curves gave the lowest coefficients of variation for all the parameters considered which indicate their suitability for use in the calculation of toughness and other fracture parameters. This confirms conclusions drawn from earlier studies on laboratory prepared test specimens.

Acknowledgements

The work reported in this paper forms part of the Brite–Euram project "Test and Design Methods for Steel Fibre Reinforced Concrete", contract no. BRPR-CT98-0813. The partners in the project are: N.V. Bekaert S.A. (Belgium co-ordinator), Centre Scientifique et Technique de la Construction (Belgium), Katholieke Universiteit Leuven (Belgium), Technical University of Denmark (Denmark), Balfour Beatty Rail Ltd. (Great Britain), University of Wales Cardiff (Great Britain), Fertig-Decken-Union GmbH (Germany), Ruhr-University-Bochum (Germany), Technical University of Braunschweig (Germany), FCC Construccion S.A. (Spain), Universitat Polytécnica de Catalunya (Spain).

The specimens tested in this investigations were prepared by Stent Foundations Ltd. and the experimental work was carried out with the assistance of Mr. Apostolos Pavlopoulos.

References

[1] Romualdi JP, Batson GP. Mechanics of crack arrest in concrete. J Eng Mech ASCE 1963;89:147–68.

[2] Swamy RN, editor. Fibre reinforced cement and concrete, Proceedings of the Fourth RILEM International Symposium. London: E&FN SPON; 1992. p. 1347.

[3] Marikunte S, Shah SP. Engineering of cement-based composites, Concrete technology—new trends, industrial applications. In: Aguado A, Gettu R, Shah SP, editors. Proceedings of the

International RILEM Workshop. London: E&FN SPON; 1994. p. 83–102.
[4] Barr B, Gettu R, Al-Oraimi SKA, Bryars LS. Toughness measurement—the need to think again. Cement Concrete Comp 1996;18:281–97.
[5] Gopalaratnam VS, Gettu R. On the characterisation of flexural toughness in FRC. Cement Concrete Comp 1995;17:239–54.
[6] Barr BIG, Hasso EBD. A study of toughness indices. Mag Concrete Res 1985;37:162–73.
[7] ACI Committee 544, Measurement of properties of fiber reinforced concrete, ACI Materials Journal 1988;85:583-593.
[8] Henegar CH. In: Toughness index of fibre concrete, testing and test method of fibre cement composites. Lancaster: RILEM Symposium Construction Press; 1978. p. 79–86.
[9] American Society for Testing and Materials, Standard method for flexural toughness and first-crack strength of fiber reinforced concrete (using beam with third-point loading) Section 4, vol. 4.02. Standard C1018-89.
[10] Johnston CD. Definition and measurement of flexural toughness parameters for fiber reinforced cocnrete. Cement Concrete Aggr 1982;4:53–60.
[11] RILEM TC 162-TDF, RILEM TC 162-TDF: Test and design methods for steel fibre reinforced concrete. Bending test. Recommendations, Materials and Structures 2000;33:3–5.
[12] Barr BIG, Taylor M, Lydon FD. Fracture toughness of high strength fibre reinforced cement composites. In: Singh G, editor. Real World Concrete Proc. R.N. Swamy Symposium, Part of Proc. Fifth CANMET/ACI International Conference on Fly Ash, Silica Fume, Slag and Natural Pozzolans in Concrete. USA: Milwaukee; 1995. p. 145–63.
[13] Taylor M, Lydon FD, Barr BIG. Toughness measurements on steel fibre-reinforced high strength concrete. Cement Concrete Comp 1997;19:329–40.
[14] Chunxiang Q, Patnaikuni I. Properties of high-strength steel fiber-reinforced concrete beams in bending. Cement Concrete Comp 1999;21:73–81.
[15] Toutanji H, Bayasi Z. Effects of manufacturing techniques on the flexural behavior of steel fiber-reinforced concrete. Cement Concrete Res 1998;28(1):115–24.
[16] Gao J, Sun W, Morino K. Mechanical properties of steel fiber-reinforced, high-strength, lightweight concrete. Cement Concrete Comp 1997;19:307–13.
[17] Mure N. Private communication from supplier of concrete piles.
[18] Norris P, Wood JGM, Barr B. A torsion test to evaluate the deterioration of concrete due to alkali-aggregate reaction. Mag Concrete Res 1990;42(153):239–44.
[19] Gere JM, Timoshenko SP. In: Mechanics of materials. third ed. Chapman & Hall; 1991. p. 158–63.
[20] Kliszczewicz A, Ajdukiewicz A. Differences in instantaneous deformability of HS/HPC according to the kind of coarse aggregate. Cement Concrete Comp 2002;24:263–7.
[21] High Strength Concrete. FIP/CEB State of the Art Report. Bulletin d'Information, No.197, August 1990.
[22] Foote RML, Mai YW, Cotterell B. Crack growth resistance curves in strain-softening materials. J Mech Phys Solids 1986; 34(6):593–607.
[23] Eissa A-B, Batson G. Model for predicting the fracture process zone and *R*-curve for high strength FRC. Cement Concrete Comp 1996;18:125–33.
[24] Ouyang C, Pacios A, Shah SP. An *R*-curve approach for pull-out of fibers from a matrix. In: Wittmann FH, editor. Fracture mechanics of concrete structures—Proceedings FRAMCOS 2. Freiburg: AEDOFICATIO Publishers; 1995. p. 783–92.
[25] Wecharatana M, Shah SP. Predictions of nonlinear fracture process zone in concrete. J Eng Mech 1983;109(3):1231–46.
[26] Bazant ZP, Gettu R, Kazemi MT. Identification of nonlinear fracture properties from size effect tests and structural analysis based on geometry-dependent *R*-curves. Int J Rock Mech Mining Sci 1991;28(1), 43–51 and 233.
[27] Banthia N, Sheng J. Fracture toughness of micro-fiber reinforced cement composites. Cement Concrete Comp 1996;18:251–69.
[28] Jenq YS, Shah SP. A two parameter fracture model for concrete. J Eng Mech Division ASCE 1985;111:1227–41.
[29] Bazant ZP, Kim J-K, Pfeiffer PA. Nonlinear fracture properties from size effect tests. J Struct Division ASCE 1986;112:289–307.
[30] Tada H, Paris PC, Irwin GR. The stress analysis of cracks handbook. Hellertown, PA: Del Research Corp.; 1985.
[31] Barr BIG, Barragán BE, Dupont D, Erdem E, Gettu R, Lee MK, Olesen JF, Schaerlaekens S, Schnütgen B, Stang H, Vandewalle L. Test methods for steel fibre reinforced concrete. Presented on August 2002 at 27th Conference of Our World in Concrete & Structures, Singapore, p. 8.
[32] Gettu R, Barragán B, Dupont D, Erdem E, Olesen JF, Rosenbusch J, Schnütgen B, Vandewalle L. Study of the parameters influencing the test results: bending and uniaxial tension tests, Report for Test and Design Methods for Steel Fibre Reinforced Concrete, EU Contract-BRPR-CT98-813, 2000. p. 196.
[33] Soroushian P, Lee C-D. Distribution and orientation of fibers in steel fiber reinforced concrete. ACI Mater J 1990;87(5):433–9.
[34] Toutanji H, Bayasi Z. Effects of manufacturing techniques on the flexural behavior of steel fiber-reinforced concrete. Cement Concrete Res 1998;28(1):115–24.
[35] Barragán BE, Gardner D, Gettu R, Ferreira LET. Study of the distribution and orientation of fibers in cast cylinders. Report for test and design methods for steel fibre reinforced concrete. EU Contract-BRPR-CT98-813, 2000. p. 8.
[36] Barr BIG, Lee MK, de Place Hansen EJ, Dupont D, Erdem E, Schaerlaekens S, Schnütgen B, Stang H, Vandewalle L. Round robin analysis of the RILEM TC 162-TDF beam-bending test: Part 3-fibre distribution. Accepted for publication by Materials and Structures 2002. p. 9.
[37] Gettu R, Barragán BE, Martín MA, Zerbino RL. A parametric study of the uniaxial tensile behaviour of steel fibre reinforced concrete. Report for Test and Design Methods for Steel Fibre Reinforced Concrete, EU Contract-BRPR-CT98-813, 2001. p. 62.
[38] RILEM TC 162-TDF, Test and design methods for steel fibre reinforced concrete. Uni-axial tension test for steel fibre reinforced concrete. Recommendations, Materials and Structures 2001;34:3–6.
[39] Barr BIG, Lee MK, de Place Hansen EJ, Dupont D, Erdem E, Schaerlaekens S, Schnütgen B, Stang H, Vandewalle L. Round robin analysis of the RILEM TC 162-TDF beam-bending test: Part 1—test method evaluation. Accepted for publication by Materials and Structures 2002. p. 22.
[40] Barr BIG, Lee MK, de Place Hansen EJ, Dupont D, Erdem E, Schaerlaekens S, Schnütgen B, Stang H, Vandewalle L. Round robin analysis of the RILEM TC 162-TDF beam-bending test: Part 2—approximation of δ from the CMOD response. Accepted for publication by Materials and Structures 2002. p. 19.
[41] Gopalaratnam VS, Shah SP, Batson GB, Criswell ME, Ramakrishnan V, Wecharatana M. Fracture toughness of fiber reinforced concrete. ACI Mater J 1991;88(4):339–53.
[42] Gopalaratnam VS, Gettu R, Carmona S, Jamet D. Characterization of the toughness of fiber reinforced concretes using the load-CMOD response. In: Wittmann FH, editor. Proceedings FRAMCOS-2. Freiburg: AEDIFICATIO Publishers; 1995. p. 769–82.
[43] Navalurkar RK, Hsu TTC, Kim SK, Wecharatana M. True fracture energy of concrete. ACI Mater J 1999;96(2):213–27.